Reconfiguration and Optimization of Lunar Navigation Satellite Constellation Targeting South Hemisphere

Shuo YANG[1,a] *, Rui ZHONG[2,b] and Franco BERNELLI ZAZZERA[1,c]

[1]Department of Aerospace Science and Technology, Politecnico di Milano, 20156 Milan, Italy

[2]School of Astronautics, Beihang University, 102206 Beijing, People's Republic of China

[a]shuo.yang@polimi.it, [b]zhongruia@163.com, [c]franco.bernelli@polimi.it

Keywords: Lunar Constellation, Constellation Reconfiguration, Multi-Objective Optimization

Abstract. The Lunar Navigation Satellite System (LNSS) is a critical initiative in response to the current surge in international lunar exploration. Compared to Global Navigation Satellite Systems (GNSS), the development of LNSS involves significantly higher costs and longer deployment cycles. As a result, optimizing constellation design to maximize the use of limited resources has become a popular topic. This work adopts two constellation reconfiguration strategies and a multi-objective optimization approach to extend the target area from the lunar South Pole to the whole Southern Hemisphere. First, Hohmann-type phasing maneuvers are applied to in-orbit satellites, with optimization of both fuel consumption and maneuver time, resulting in a notable improvement in dual coverage performance over the South Hemisphere. Second, new satellites are introduced to restore high-quality service in the South Pole region. Simulation results of coverage and navigation performance at the lunar South Pole confirm the effectiveness of the final constellation scheme.

Introduction

In 2005, NASA proposed six lunar communication architectures, regarding the resource-rich lunar south pole as the first exploration target [1]. In recent years, many studies have focused on the configuration design of lunar constellations. For example, Circi et al. used Halo orbits around L1 and L2 libration points to build a lunar constellation [2]. Zanotti et al. performed a multi-objective optimization of lunar orbits, targeting both low-altitude orbital missions and surface operations near the lunar South Pole [3].

The deployment of medium and large constellations usually involves reconfiguration operations, which are mainly applied in two scenarios. The first application scenario occurs when a satellite experiences an anomaly or a loss of functionality. Ferringer et al. simulated two failure scenarios and employed an evolutionary algorithm to optimize the reconfiguration process [4]. Arnas and Linares proposed a reconfiguration strategy considering the constraint of minimum inter-satellite safety distance [5]. The second scenario is the phased constellation deployment. Oliver et al. employed an Auction algorithm to derive the optimal assignment of satellites [6]. Alexandra et al. explored the design of a reconfigurable Earth observation satellite constellation, significantly improving detection rates for ground events [7].

In previous research, satellite constellations targeting the lunar South Pole have been optimized and analyzed [8]. This paper first presents the phase maneuvering methods, then the optimization models for two reconfiguration phases, followed by the results and conclusions.

Orbital Phasing Maneuver

The first-phase reconfiguration is intended only as a temporary response to the urgent navigation demands in the Southern Hemisphere. Therefore, only orbital phase is adjusted. A Hohmann-type phasing maneuver is employed, including a sub- and a super-synchronous transfer, illustrated respectively in Fig. 1(a) and Fig. 1(b).

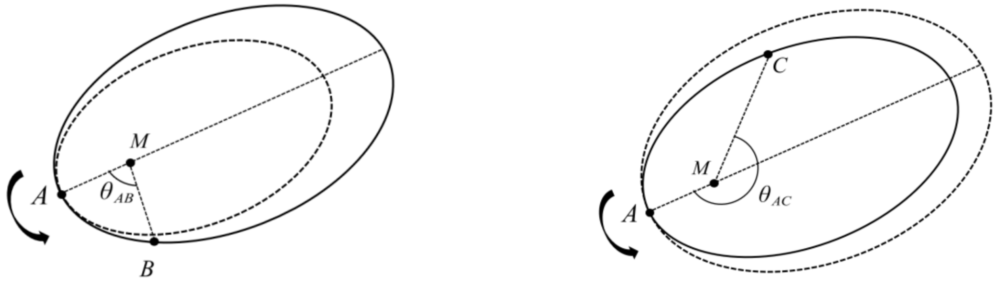

(a) *Sub-synchronous transfer* (b) *Super-synchronous transfer*

Figure 1: Phasing maneuver strategies. M denotes the Moon, A represents the perilune, and B and C indicate the target positions.

When the phase angle between the target position and the perilune satisfies $\theta_{AB} \leq 180°$, the sub-synchronous transfer is performed. The satellite enters a transfer orbit with lower attitude applying an impulse in the direction opposite the velocity at the perilune. After completing an integer number of revolutions, the satellite returns to original orbit using an equal impulse. Define t_{AB} as the time taken to move from A to B along the original orbit. Then the period of the transfer orbit can be calculated by

$$T_{sub} = T_0 - \frac{\Delta t_{AB}}{W} \tag{1}$$

where T_0 presents the period of the original orbit, and W represents the number of revolutions in the transfer orbit. The total velocity increment Δv_1 of two maneuvers can be given by

$$\Delta v_1 = 2|v_{Asub} - v_{A0}| \tag{2}$$

where v_{Asub} and v_{A0} represent the velocities of the perilune in the transfer orbit and the original orbit, respectively. The total duration of the transfer process is

$$\Delta t_1 = W \cdot T_{tran1} \tag{3}$$

When the phase angle satisfies $\theta_{AC} > 180°$, the super-synchronous transfer is employed. In this case, the satellite requires an accelerating impulse to change to a higher-altitude transfer orbit. Define t_{AC} as the time taken to move from A to C along the original orbit. Then, the period of the transfer orbit is

$$T_{super} = \frac{W+1}{W} T_0 - \frac{\Delta t_{AC}}{W} \tag{4}$$

The velocity increment Δv_2 and transfer duration Δt_2 can be determined in the same way as the previous case.

Optimization Model

Optimization Variables.

In the initial step of the reconfiguration, only the phases need to be adjusted. Therefore, the optimization variables and their bounds are

$$x_{\mathrm{SH1}} = (\theta_i, W_i)^T, i = 1,2,\cdots, N_{\mathrm{SP}},$$
$$x_{\mathrm{SH1}lb} = (0° \times N_{\mathrm{SP}}, 1 \times N_{\mathrm{SP}})^T, x_{\mathrm{SH1}hb} = (360° \times N_{\mathrm{SP}}, 3 \times N_{\mathrm{SP}})^T \quad (5)$$

where N_{SP} denotes the number of satellites in previous research [8].

In the second phase, the optimization focuses on orbital parameters of the new satellites. Consequently, both the orbital inclinations $incline_i$ and eccentricities e_i are considered as independent variables, and the allowable range for the perigee arguments ω_i is extended.

$$x_{\mathrm{SH2}} = (incline_i, e_i, \omega_i, \Omega_i, \theta_i)^T, i = 1,2,$$
$$x_{\mathrm{SH2}lb} = (0° \times N_{\mathrm{SH}}, 1 \times N_{\mathrm{SH}})^T, x_{\mathrm{SH2}hb} = (360° \times N_{\mathrm{SH}}, 3 \times N_{\mathrm{SH}})^T \quad (6)$$

where Ω_i and θ_i represent the right ascension of the ascending node and the true anomaly, respectively.

Objective Functions.

Two coverage performance metrics $Cov2_i$, $Cov4_i$, and two navigation performance metrics $PerHDOP_i$, $PerGDOP_i$ are applied. Denote SP as the region spanning latitudes 70°S to 90°S, while SH as the region from 0°S to 70°S. In the phasing maneuver stage, the fuel consumption and reconfiguration time are also included as optimization objectives. As a result, there are seven optimization objectives for the first phase: $Cov4_{\mathrm{SP}}$, $PerHDOP_{\mathrm{SP}}$, $PerGDOP_{\mathrm{SP}}$, $Cov2_{\mathrm{SH}}$, $Cov4_{\mathrm{SH}}$, $\sum \Delta v_i$, $\max(\Delta t_i)$. The objective functions for the second phase are $Cov4_{\mathrm{SP}}$, $PerHDOP_{\mathrm{SP}}$, $PerGDOP_{\mathrm{SP}}$, $Cov2_{\mathrm{SH}}$, $Cov4_{\mathrm{SH}}$, $PerHDOP_{\mathrm{SH}}$.

Results

The optimization is based on two constellation schemes designed for lunar SP region in previous work, whose performance metrics are listed in Table 1.

Table 1: Performance metrics of constellation schemes targeting South Pole

Schemes	$Cov4_{\mathrm{SP}}$	$PerHDOP_{\mathrm{SP}}$	$PerGDOP_{\mathrm{SP}}$	$Cov2_{\mathrm{SH}}$	$Cov4_{\mathrm{SH}}$
SP_E	100%	91.03%	49.02%	61.23%	0%
SP_F	100%	94.91%	67.53%	80.73%	0%

The NSGA-II (Elitist Non-dominated Sorting Genetic Algorithm) method is used to optimize the model in last section. The sub-Pareto fronts are shown in Fig. 2. Compared to Table 1, most of the solutions in Fig. 2(a) and Fig. 2(b) no longer satisfy the continuous four-fold coverage over SP. Additionally, the navigation performance exhibit significant degradation. Solutions SH1_A and SH1_B in Fig. 2(c) achieve the highest $Cov2_{\mathrm{SH}}$ while maintaining 100% $Cov4_{\mathrm{SP}}$. However, the improvement in $Cov2_{\mathrm{SH}}$ compared to SP_E and SP_F is marginal, and the $PerGDOP_{\mathrm{SP}}$ deteriorates by over 15%. Similarly, solutions SH1_C and SH1_D in Fig. 2(d) reach the highest $Cov4_{\mathrm{SH}}$ while also ensuring 100% $Cov4_{\mathrm{SP}}$. But their $Cov2_{\mathrm{SH}}$ drops by more than 28%, and the navigation performances for SP are severely compromised. It is evident that none of these four representative points can be considered as the final solutions. Fig. 2(e) illustrates an inverse correlation between $Cov2_{\mathrm{SH}}$ and $Cov4_{\mathrm{SH}}$. Dual coverage is the most urgent requirement in the first

Materials Research Proceedings 69 (2026) 1140-1145 https://doi.org/10.21741/9781644904251-196

stage, so solution SH1_E with the highest $Cov2_{\mathrm{SH}}$ is selected. As shown in Fig. 2(f), the velocity increment remains below 0.25 km/s, and the maximum maneuver duration does not exceed 83 hours, which is a positive outcome in terms of both efficiency and energy consumption.

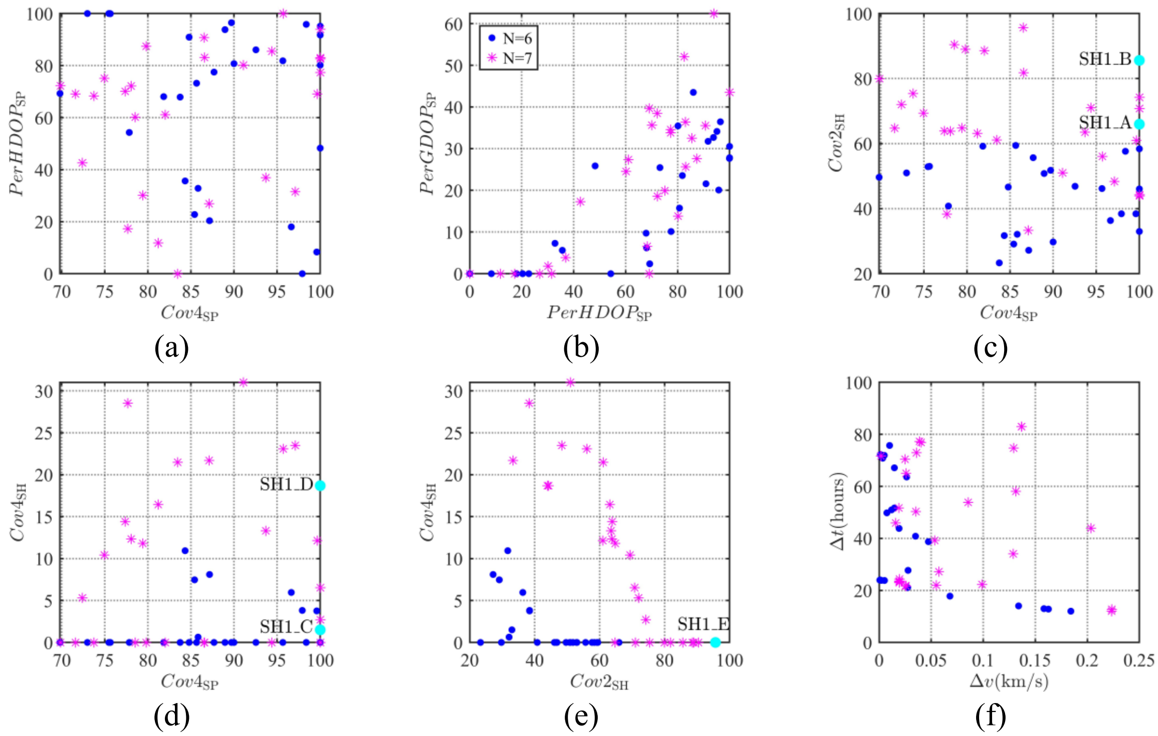

Figure 2: The Optimization Pareto fronts of the first stage of reconfiguration. N represents the number of the satellites.

The performance metrics of solution SH1_E $Cov4_{\mathrm{SP}}$, $PerHDOP_{\mathrm{SP}}$, $PerGDOP_{\mathrm{SP}}$, and $Cov2_{\mathrm{SH}}$ are 86.52%, 90.74%, 35.53%, and 95.66%, respectively. It can be observed that SH1_E exhibits performance decline over the SP region compared to SP_F. Therefore, in the second phase, the new satellites are added to restore the performance in SP regions. The second sub-Pareto fronts are illustrated in the Fig. 3. As seen in Fig. 3(a) and Fig. 3(b), significant improvements are observed in the performances for SP region. According to Fig. 3(c), the $Cov2_{\mathrm{SH}}$ of all solutions maintains no lower than 95.66%. By comparing five candidate solutions satisfying 100% $Cov4_{\mathrm{SP}}$ and better $PerHDOP_{\mathrm{SP}}$ than SP_F, scheme SH2_A with highest $PerGDOP_{\mathrm{SP}}$ and $PerHDOP_{\mathrm{SH}}$ is chosen as the final solution.

To evaluate the service capability, the coverage and navigation performance at the South Pole are shown in Fig. 4. From Fig. 4(a), it can be seen that the coverage redundancy at the south pole always exceeds five-fold, which implies superior navigation performance. This is further validated by Fig. 4(b). During the 10-day simulation period, the HDOP at the south pole remains below 5, while the GDOP stays below 10 for the most of time. These values indicate that scheme SH2_A can provide precise navigation support for most lunar missions at South Pole.

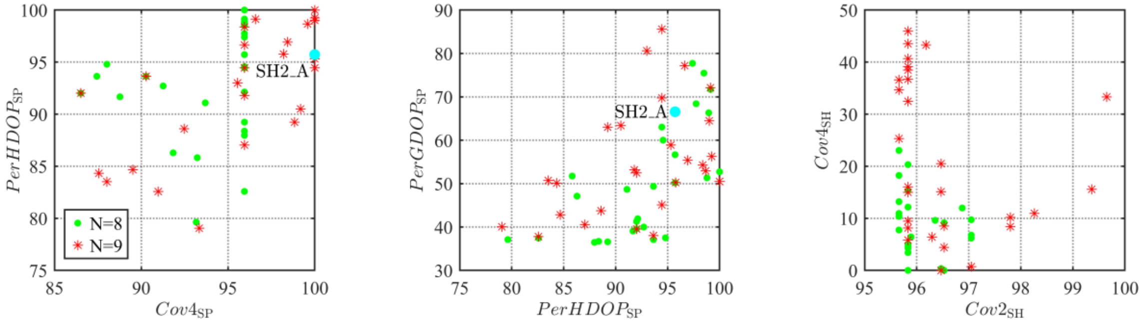

(a) (b) (c)

Figure 3: The Optimization Pareto fronts of the second stage of reconfiguration. Only three sub-Pareto fronts are shown here. N=8 and N=9 represent the addition of one or two satellites, respectively.

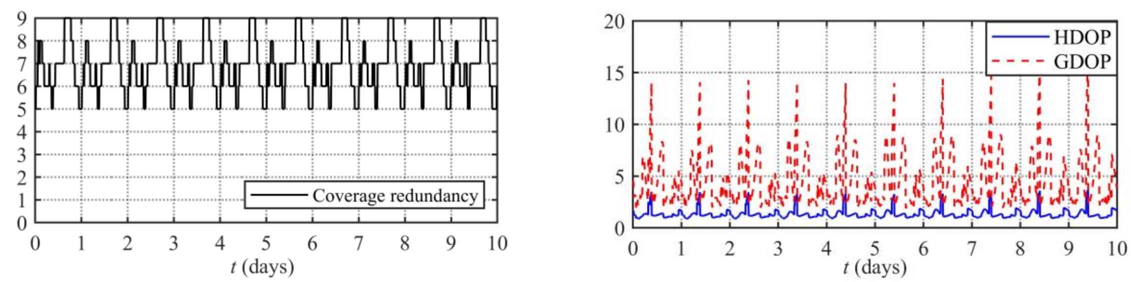

(a) *Coverage redundancy at South Pole.* (b) *HDOP and GDOP at South Pole.*

Figure 4: Coverage and navigation performance of SH2_A at South Pole. The simulation time is chosen as 10 days.

Conclusion

Based on the constellation schemes targeting the South Pole, this work applies the reconfiguration to extend the service area to the entire Southern Hemisphere. In the first stage, Hohmann-type phasing maneuvers are employed to adjust the phases of in-orbit satellites, with optimization for minimizing fuel and time consumption. Selected scheme SH1_E is able to achieve over 95% dual coverage across the Southern Hemisphere. In the second stage, one to two new satellites in non-frozen orbits are deployed to restore continuous four-fold coverage over the South Pole region.

Acknowledgments

This work was supported by the China Scholarship Council (CSC).

References

[1] K. Bhasin, A. Hackenberg, R. Slywczak, P. Bose, M. Bergamo, J. Hayden, Lunar relay satellite network for space exploration: architecture, technologies and challenges, in: 24th AIAA International Communications Satellite Systems Conference, AIAA, San Diego, California, 2006, p. 5363. https://doi.org/10.2514/6.2006-5363

[2] C. Circi, D. Romagnoli, F. Fumenti, Halo orbit dynamics and properties for a lunar global positioning system design, Monthly Notices of the Royal Astronomical Society. 442 (2014) 3511-3527. https://doi.org/10.1093/mnras/stu1085

[3] G. Zanotti, M. Ceresoli, A. Pasquale, J. Prinetto, M. Lavagna, High performance lunar constellation for navigation services to moon orbiting users, Advances in Space Research. 73 (2024) 5665-5679. https://doi.org/10.1016/j.asr.2023.03.032

Materials Research Proceedings 69 (2026) 1140-1145 https://doi.org/10.21741/9781644904251-196

[4] M. Ferringer, D. Spencer, R. Clifton, T. Thompson, P. Reed, Pareto-hypervolumes for the reconfiguration of satellite constellations, in: AIAA/AAS Astrodynamics Specialist Conference and Exhibit, AIAA, Honolulu, Hawaii, 2008, p. 6611. https://doi.org/10.2514/6.2008-6611

[5] D. Arnas, R. Linares, Uniform satellite constellation reconfiguration, Journal of Guidance, Control, and Dynamics. 45 (2022), 1241-1254. https://doi.org/10.2514/1.G006514

[6] O.L. De Weck, U. Scialom, A. Siddiqi, Optimal reconfiguration of satellite constellations with the auction algorithm, Acta Astronautica. 62 (2008), 112-130. https://doi.org/10.1016/j.actaastro.2007.02.008

[7] A.N. Straub, D.E. Hastings, D.W. Miller, O.L. De Weck, Deployment strategies for reconfigurable satellite constellations, in: ASCEND 2020, AIAA, VirtualEvent, 2020, p. 4246. https://doi.org/10.2514/6.2020-4246

[8] S. Yang, R. Zhong, Optimization method for lunar navigation satellite constellation targeting south pole, in: L. Yan, H. Duan, Y. Deng (Eds.), Advances in Guidance, Navigation and Control, Springer Nature Singapore, 2025, pp. 495-504. https://doi.org/10.1007/978-981-96-2248-1_48